The Structure of Herbig-Haro Object 43

and

Orion Dark Cloud Extinction

Richard D. Schwartz[1]

Department of Physics

University of Missouri, St. Louis

Michael A. Dopita

Mount Stromlo and Siding Spring Observatories

Research School of Physical Sciences

Australian National University

Martin Cohen

NASA-Ames Research Center

and

Radio Astronomy Laboratory

University of California, Berkeley

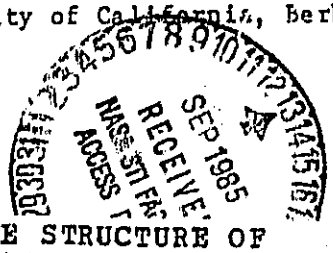

[1] Guest Investigator with NASA's International Ultraviolet Explorer (I.U.E.) Telescope.

Abstract

New ultraviolet and optical observations of Herbig-Haro Object No. 43 are reported. Continuum and emission-line fluxes in the range 1250Å<λ<7350Å have been measured. The continuum fluxes are best matched by an enhanced H^0 two-photon component added to H^0 free-bound emission, assuming a θ Ori extinction curve with $E(B-V) = 0.2$, $R = 5$. The structure and dynamics of three components within the object are discussed. The object has a radiative output of $> 0.23\ L_\odot$ in ultraviolet and optical radiation combined. The energy requirements are discussed in terms of the production of shock waves by a collimated, supersonic mass outflow from a nearby infrared source.

I. Introduction

The low-excitation Herbig-Haro (HH) Object No. 43 (= Haro 14a) has been the subject of several optical spectrophotometric studies (Dopita, Binette, and Schwartz 1982; Böhm, Brugel, and Olmsted 1983). Dopita et al. (1982) first hypothesized the character of the blue-ultraviolet continuum "excess" as being due to enhanced H° two-photon (2q) emission in a relatively low-velocity shock. Schwartz (1983) obtained ultraviolet spectrophotometry of the object in the range λλ 1250-2000Å, finding evidence of the continuum maximum near λ1500Å predicted by the 2q hypothesis, as well as the presence of Lyman band H_2 emission lines produced by fluorescence with H° Lyman α.

In this paper we report the results of new ultraviolet spectrophotometry of HH 43 in the range λλ 1250-3100Å, and new optical spectrophotometry in the range λλ 3500-7350Å. In combination with the results of Dopita et al. (1982) and Schwartz (1983), the new data are analyzed to determine the form of the interstellar extinction correction for HH 43. The continuum and emission line fluxes, corrected for extinction, are then used to discuss the energetics and shock wave dynamics of this object.

II. Observations and Results

a) Ultraviolet

The International Ultraviolet Explorer (I.U.E.) was employed on 1984 August 22 to obtain an ultraviolet spectrum of HH 43 with the short wavelength prime (SWP) camera at low dispersion. The exposure of 425 min duration covering the range λλ 1200-2000Å, was carried out with the same spectrograph

settings as the 1982 exposure of HH 43 which had a duration of 390 min (Schwartz, 1983). The I.U.E. long wavelength prime (LWP) camera was used on 1984 August 19 in a 420 min. exposure to obtain a spectrum of HH 43 in the wavelength range λλ 2000-3100Å. In all exposures the large aperture (approximately 10."3 x 23" elongated figure) was used with a position angle of 146°. The long axis of HH 43 is aligned in position angle 135° which permitted the entire object (~15" long) to be observed through the aperture (see Figure 1).

An extended source reduction was carried out for each spectrum as described in Turnrose, Harvel, and Stone (1981). The geometrically and photometrically processed images were reprocessed at the I.U.E. Regional Data Analysis Facility at the Goddard Space Flight Center. Each spectrum was subjected to 3-point smoothing prior to emission-line and continuum flux measurements.

Emission lines were identified and measured as in the earlier work (Schwartz 1983). The results of the UV emission line measurements are presented in table 1 (columns 3 and 4) for both the 1982 and the 1984 spectra. The questionable C II λ 1335.9 line which was noted in the 1982 SWP spectrum was not present in the 1984 SWP spectrum, therefore it was likely the result of a cosmic ray "hit". However, the lines of the H_2 Lyman band, produced by fluorescence with H° Lyman α, are present on both the 1982 and 1984 spectra, and the lines exhibit about the same strengths (see Schwartz 1983 for a display of the SWP spectrum). The extinction-corrected mean relative intensities of the H_2 lines (Column 7) agree favorably with those predicted by Dopita's (unpublished) theoretical calculations (Column 8). The LWP spectrum, displayed in Figure 2, was found to exhibit emission lines of C I], C II], [O II], and Mg II as expected in a low-excitation nebula.

Continuum fluxes were measured by computing the mean flux in 50Å wide bins at 50 Å intervals. For bins containing identified emission lines, the emission line fluxes were subtracted to yield continuum levels. The integrated flux of the 1982 SWP spectrum agrees to within 10% of the integrated flux of the 1984 SWP spectrum, although a few wavelengths differ by as much as 50% in their continuum strengths between the two exposures. This is indicative of the rather low signal in this faint object (eg., in the λλ 1300-1500Å region the binned fluxes typically have standard deviations of ~40%). Since the integrated fluxes indicate that little if any variation occurred in this object over the two year period, the continuum fluxes contained in table 2, column 3, have been obtained by simple averaging of the 1982 and 1984 results. The continuum points for the range $2000 \leq \lambda \leq 3100$Å are the result of the single LWP spectrum described above. It should be noted that the SWP continuum fluxes in the range λλ 1800-1950Å extrapolate to reasonable agreement with those obtained with the LWP camera in the range λλ 2000-2300.

b) Optical

New spectrophometry of HH 43 was obtained on the night of 1984 April 2-3 using the Anglo-Australian 3.9 m telescope. The 25 cm camera of the Royal Greenwich Observatory Spectrograph was used with the Image Photon Counting System (IPCS) (Boksenberg 1972) as detector. Spectrograph settings identical to those used in the 1981 January 8-9 observation of HH 43 were employed (Dopita et al. 1982). A 250 lines mm^{-1} grating was used in first order with a slit of 400 μm (2."65 on the sky), yielding a resolution of 11 Å in the spectral range $3400 \leq \lambda \leq 7500$ Å. The external memory was used to give 50 spectra, each 2044 pixels long, separated by 2."07 on the sky. The data

reduction procedure was identical to that described in Dopita et al. (1982), and the reader is referred to that work for a more detailed account of the data reduction and the spectrophotometric accuracy of the system.

In observing HH 43, a position angle of 135° was used in both the 1981 and 1984 measurements. With the slit aligned with the long axis of the object, three separate regions of the object could be readily identified (see Figure 1). Component A filled two pixels (~4") along the slit; component B filled four pixels (~8"); and component C filled 3 pixels (~6"). Regions to the NW and SE of HH 43, clearly free of emission from the object, were used for sky subtraction. In the 1981 observations (Dopita et al. 1982), the emission-line and continuum fluxes from all three components were summed and tabulated as an averaged spectrum for the entire object. With the new data, we present the relative emission-line intensities separately for the three components in columns 3-5 of table 3. From the H_β flux tabulated near the bottom of each column, one notes that indeed component B is the brightest of the three, whereas component A is the faintest. Figure 3 presents the spectrophotometric tracings for the three components of HH 43 from the 1984 spectrum, corrected to above-atmosphere fluxes. There is a striking difference in the excitation level of component A as compared with B and C. Whereas 43A exhibits prominent [O III] λ 5007 emission, components B and C show no detectable [O III] emission. At the same time, [N I] λ 5200 is very strong in components B and C, and very weak in A. Also, a large velocity gradient is evident from A to C as shown by the (heliocentric) radial velocities in table 3. The velocities have been measured relative to night sky emission lines which fill the length of the slit.

Table 3 includes a summary of the emission line fluxes from both the 1981 and 1984 observations. Columns 6 and 7, respectively, give the fluxes summed over the three components for each of the observations. A systematic difference is evident in the sense that the emission-line intensities longward of H_β are less in the 1984 spectrum than in the 1981 spectrum, and the reverse circumstance holds for lines shortward of H_β. In obtaining the intensities normalized to $F(H_\beta)$ for each spectrum, a standard set of atmospheric extinction coefficients (mean coefficients for the A.A.T. site) was used. Whereas both the 1981 and 1984 observations were made on cloudless nights, the presence of smoke layers was noted on the night of the 1984 observations. We suspect that this may have had the effect of creating a more neutral extinction, thus by (incorrectly) using the mean coefficients, the blue fluxes were overcorrected relative to the red fluxes. Without an independent calibration of the extinction on each night, however, we are unable to confirm this suspicion. Considering that the 1984 fluxes are probably less certain owing to the smoke layers, we have given the 1981 fluxes double weight in arriving at the average emission-line intensities listed in column 8.

For optical continuum measurements, regions as free of emission lines as possible were chosen (see Dopita et al. 1982). Again, in comparing the 1981 and 1984 fluxes, it was found that the 1984 red continuum fluxes appeared to be undercorrected relative to the blue fluxes by approximately the amount found in the emission lines. In arriving at mean optical continuum fluxes given in table 4, again double weight was given to the 1981 observations.

The absolute optical spectrophotometry obtained through the 2."6 slit cannot be compared directly with that obtained with the I.U.E. (which measured the entire object). In order to normalize the optical data to the UV data, it was assumed that the continuum followed the combined H° two-photon plus free-bound (f-b) spectrum found by Dopita et al. (1982). After correcting the continuum data points for a particular value of reddening (see section II c), the UV continuum fluxes in the range $2700 < \lambda < 3100$ Å (where the UV flux uncertainties are minimal) were fit to the theoretical 2q plus f-b spectral energy distribution. The optical fluxes ($\lambda > 3390$ Å) were then adjusted upward by a common factor to achieve a best fit to the theoretical energy distribution. For the reddening which was finally adopted ($E_{B-V} = 0.2$, Θ Ori extinction), the optical fluxes had to be increased by a factor of 1.83. This suggests that about 55% of the total optical light from HH 43 was measured through the 2."6 slit. The H_β flux at the bottom of column 8 in table 3 and the continuum fluxes in column 3 of table 4 represent the best adjusted estimate for optical fluxes from the entire object. In adjusting the optical fluxes to achieve normalization with the UV fluxes, we have made the assumption that the emission-line and continuum emitting regions are co-extensive over the face of HH 43.

c) Extinction Corrections

Böhm, Brugel, and Olmsted (1983) measured the intensities of the [S II] λ 10317/10336 and λ 4068/4076 lines in HH 43, and applied Miller's (1968) method for the reddening correction along with the assumption of a normal interstellar reddening curve to find $E(B-V) = 0.46$. Correcting our continuum fluxes in tables 2 and 4 for "normal" (Savage and Mathis 1979) extinction using $E(B-V) = 0.46$ yields the results plotted in Figure 4. The solid curve

represents the combination of two-photon and free-bound emission found by Dopita et al. (1982), whereas the dashed-line component represents two-photon emission only. In normalizing the theoretical curve to the observed near-UV fluxes ($3500 < \lambda < 4000$ Å), it is seen that the fit is very poor throughout the remainder of the spectrum. The "normal" extinction curve assumes a ratio of total to selective extinction of 3.1.

It has become increasingly evident that a peculiar extinction curve is required for many HH objects (see Böhm and Böhm-Vitense 1984, and references therein). The logical choice, especially for objects in the Orion dark cloud complex, is the mean extinction curve derived for the Θ Ori stars by Bohlin and Savage (1981). Although the peculiar Θ Ori extinction is essentially identical to "normal" extinction in its relative wavelength dependence in the range $4400 < \lambda < 6000$ Å, there are large differences between of the two curves in the UV range in the sense that Θ Ori extinction tends to be relatively neutral. Also, from the measurements of Lee (1968), there is an indication that the Θ Ori extinction becomes greater in the red and near-infrared than does normal extinction, signaling the effect of a larger ratio of total to selective extinction. This effect is presumably due to the presence of larger grains in the dark cloud than in the diffuse interstellar medium. Assuming a ratio of total to selective absorption of 5, we have corrected the observed fluxes using Θ Ori extinction for $E(B-V) = 0.46$, with the results plotted in Figure 5. Although the fit to the theoretical 2q plus f-b curve is much better than in Figure 4, there remain significant departures between the observed points and the theoretical curve in the ranges $2000 < \lambda < 2650$ Å and $\lambda > 5470$ Å.

Dopita et al. (1982) used a reddening correction procedure which involved the ratio R defined by

$$R = \frac{I(6717+6731)}{I(4068+4076)} \cdot \frac{I(7318+7328)}{I(3727+3729)}$$

From a large series of theoretical shock wave models produced over a wide range of pre-shock densities and post-shock temperatures, it was found that this ratio was reasonably predictable as a function of electron density (i.e., as reflected by the $\lambda 6731/\lambda 6717$ intensity ratio). Thus the observed value of R, in combination with the theoretical value predicted for the observed n_e, yields an estimate of the reddening in the range $3720 < \lambda < 7330$Å. Assuming normal extinction in this range, Dopita et al. found a logarithmic extinction at H_β of C = 0.3, corresponding to E(B-V) = 0.2. We have used this value of the selective extinction and the Θ Ori extinction curve with a ratio of total to selective extinction of 5 to correct the continuum fluxes in HH 43. These results are plotted in Figure 6 where it is seen that the observed fluxes now are fit remarkably well by the 2q plus f-b theoretical curve. We have adopted this form of the extinction to compute the corrected fluxes which appear in tables 1-4.

III. Discussion

a) Orion Dark Cloud Extinction

Within the uncertainties of the observational data, we have concluded that a Θ Ori extinction curve with E(B-V) = 0.2 is most appropriate for HH 43. Examination of Figure 6 suggests that continuum fluxes may have been overcorrected in the range $(1/\lambda)$ 4.76-4.44 μm^{-1}. This would indicate that the

graphite 2175 Å ($4.60\ \mu m^{-1}$) absorption feature is less prominent than for the Θ Ori stars, although the large flux uncertainties in that wavelength region for HH 43 render this conclusion somewhat speculative. In Figure 7 we present the normal (Savage and Mathis) and Θ Ori (Bohlin and Savage) extinction curves normalized to E(B-V) = 1.0. The dashed line in the $\lambda\lambda$ 2000-2500Å region of the Θ Ori curve is suggestive of a form of the extinction which would improve the fit in that region for the data points in Figure 6.

In addition, in Figure 7 we have located the relative extinction at λ 1.0317 μm as implied from the measurements of Böhm et al. (1983), normalized to E(B-V) = 1.0. An extrapolation from the optical fluxes through this point suggests that the ratio of total to selective extinction is R > 4.5. The adopted value of R = 5 is obviously somewhat arbitrary. With the uncertainty as indicated in the λ 10317/λ4072 [S II] fluxes, added to the extrapolation to $(1/\lambda) = 0$, it is evident that R could fall anywhere in the range 4 - 8. In terms of absolute extinction at H_β(λ4861) for E(B-V) = 0.2, this range for R corresponds to flux corrections from a factor of 2.3 (for R = 4) to 4.8 (for R = 8). In principle, measurements of the thermal radio flux in combination with the H_β flux could be used to obtain more points on the extinction curve very close to $1/\lambda = 0$. However, the interpretation of the radio and H_β fluxes would be somewhat model-dependent in the sense that HH 43 is not a classical H II region, but rather the product of shock waves covering a range of shock velocities. Moreover, the low-excitation character of this object indicates that the ionization state, on the average, is relatively low. In comparison with HH 1 and 2 (high excitation HHs which have recently been detected at the 1 mJy level by Pravdo et al. 1985), it is evident that HH 43 is probably well below the detection limit for present radio telescopes.

On the basis of extinction determinations for individual knots within HH 1, Hartmann and Raymond (1984) concluded that large differential extinction exists over small spatial scales (~3"). Munch (1983) has argued that much of the extinction may be due to internal dust within the HH objects. It is of some interest to explore the implications of such a proposal for the extinction found in this work for HH 43.

First, we can estimate the optical depth at λ5550Å for absorbing material <u>if it is entirely external</u> to the emitting regions in the HH object. Since for this case

$$F = F_o \, e^{-\tau_V} \, .$$

where F is the observed flux and F_o is the extinction corrected flux, for a ratio of total to selective extinction of 5, our value of E(B-V) = 0.2 implies $A_V = 1.0$, or $\tau_V = 0.92$. For the case in which the extinction would occur entirely internal to the HH object with dust mixed uniformly with the emitting gas, one has

$$F = \frac{F_o}{\tau_V} (1-e^{-\tau_V})$$

For the visual extinction of 1 mag which produces $F = 0.4 \, F_o$, one finds that $\tau_V = 2.2$ for this case. For a characteristic column depth of emitting gas in HHs of 10^{16} cm, one can arrive at an estimate of the dust to gas ratio required to produce 1 mag of internal extinction if the approximation for extinction by relatively large grains is used,

$$\tau_V = \kappa_V \ell = \sigma n_g \ell$$

where σ is the geometrical cross section for the average grain, n_g is the grain number density, and ℓ is the column depth. For an average grain radius of 0.1 μm, $\tau_V \approx 2.2$ requires that $n_g \approx 7 \times 10^{-7}$ cm^{-3}. For a grain mass density of 3 g cm^{-3} and a typical HH (post-shock) gas density of 10^4 cm^{-3}, this results in a dust to gas ratio of $\sim$0.5. Moreover, the use of larger grains exacerbates the problem. For an average grain radius of 0.3 μm the calculation leads to a dust to gas ratio of 1.3. Even though our estimates have been generated with coarse approximations, it seems unlikely that any combination of parameters can be changed to lower the dust to gas ratio to the more conventional value of $\sim$0.01. We conclude that most of the extinction is likely due to dust which is external to the HH object, but still internal to the dark cloud complex in which the object is embedded. Within the uncertainties of the continuum and emission line fluxes in the individual components 43B and 43C, we find no difference in the relative extinction between these knots. (The fluxes from 43A are too low for a meaningful analysis.)

b) Structure and Dynamics

Cohen and Schwartz (1983) reported discovery of an embedded 2 μm infrared source (IRS 1) approximately one arc min NW of HH 43 as indicated in Figure 1. The region was surveyed on the basis of proper motion measurements by Jones (Private Communication) which indicated a motion of components 43 B and C relative to 43 A in the direction of the long axis of the object. It was suggested that components B and C are moving to the SE and thus that the exciting star should be located to the NW of HH 43. In addition, the fainter, more diffuse object HH 38 is located about 3 arc min SE of HH 43, and may represent an older part of the collimated mass flow from IRS

1. Far-infrared photometry of IRS 1 (Cohen et al. 1984) in combination with near-IR and mid-IR measurements yields a bolometric luminosity of ~ 5 $L_\odot$ for the star.

Curiously, the excitation structure of HH 43 appears to be the reverse of that for HH 1 when viewed with respect to the exciting star. In HH 1, the low-excitation portion of the nebula is "trailing" (i.e., closer to the exciting star), with the high-excitation component forming the leading edge. This is suggestive of the "interstellar bullet" model for HHs (Norman and Silk 1979) in which a fragment is plowing supersonically into the ambient medium. In HH 43, the high excitation component (A) is facing IRS 1, with the low-excitation parts (B and C) lying further from the star. This might be produced by a collimated stellar wind infringing upon an obstacle cloudlet as proposed in Schwartz's (1978) model.

The [S II] λ 6717/6731 emission-line ratio reveals a prominent increasing density gradient from 43 A to C. The low density ($n_e < 200$ cm^{-3}) for 43 A probably accounts for its relatively low luminosity, whereas the higher density (and larger volume) components B ($n_e \sim 700$ cm^{-3}) and C ($n_e \sim 2000$ cm^{-3}) are seen to dominate the optical image. The average electron density ($n_e \sim 700$ cm^{-3}) of HH 43 is somewhat lower than that found for other HHs, and this may be a factor in the relatively low intensities for lines of Ca II, Mg I], Mg II, and [Fe II].

The velocity gradient from HH 43 A to 43 C behaves in a fashion which is consistent with the proper motion measurements. Evidently, component A is quasi-stationary, feeling the full brunt of the mass flow which produces a

high-excitation shock wave. Material in B and C appears to be moving away from the star with a component of motion toward earth. It is tempting to look upon HH 43 as the product of an inhomogeneous, elongated bow-shock. The arcuate structure of 43 A seen on photographs is indicative of the head of a bow-shock where maximum temperatures will prevail. Components 43 B and C would represent portions of the flow passing through a distended, oblique portion of the bow wave. The result is a lower shock velocity and temperature (only the velocity component normal to the oblique front contributes to heating) with a substantial velocity of the shocked material since the velocity component parallel to the oblique front is unaffected by shock passage. The collimated flow would itself have to possess density inhomogeneity in order to account for the density structure in HH 43.

Dopita et al. (1982) concluded that the object may be dominated by a non-equilibrium shock in which a substantial recombination zone has not yet developed. This has the effect of enhancing the $2q/H_\beta$ ratio because of the dominance of collisional excitation prior to the development of a recombination zone. Enhancement of 2q emission occurs also in a low-velocity shock since only a small fraction of the hydrogen entering the shock may in fact be ionized after passage through the shock. Relative to its H_β flux, HH 43 A exhibits extremely weak continuum (Figure 3a), a feature indicative of higher velocity shocks in which the post-shock hydrogen is completely ionized. By contrast, the low-excitation components B and C show very obvious continua increasing toward shorter wavelengths (Figures 3 b,c), confirming the intimate connection between low-velocity shocks and the 2q enhancement.

c) Energy Considerations

Assuming a distance of 460 pc for HH 43, it is possible to compute the luminosity of the object from the information in tables 1-4. For all observed emission lines we find L(lines) = 0.055 $L_\odot$, and for the integrated UV and optical continuum we find L(cont) = 0.177 $L_\odot$, giving a total L = .23 $L_\odot$. This is a lower limit for the luminosity since it omits Lyman line fluxes and infrared emission lines. The shock wave model which was used to synthesize the spectrum of HH 43 (Dopita et al. 1982) indicates that atomic transitions will probably not contribute a substantial amount of flux in the infrared. The [O I] λ 63 μm line, for example, is predicted to have I = 110 (relative to $I_{H\beta}$ = 100) from the optical nebula, and the Si II λ 34.8 μm may be somewhat stronger at I = 622. This may be an overestimate since the shock model also predicts I = 1480 for the Mg II λ 2800 lines, 18 times greater than observed! It is possible that heavier elements (Ca, Mg, Si, Fe, etc.) are significantly depleted in the gas phase (i.e., they are tied up in grains) in HH 43. More important is the potential IR emission from warm H_2. The UV H_2 Lyman band emission requires that H_2 be warmed to the v" = 2, j" = 5 vibrational level of the ground state $X^1\Sigma_g^+$ in order for Lyman α pumping to the $B^1\Sigma_u^+$, v' = 1, j' = 4 level to occur, from which springs the particular series of lines listed in Table 1. The v" = 2 level of ground state H_2 is thought to be populated by collisions in warm (2000-3000K) shocked gas, and the characteristic infrared lines S(2) 2.15 μm, S(1) 2.12 μm, and Q(3) 2.42 μm are produced as transitions occur to lower vibrational and rotational levels. It would be of great interest to observe HH 43 in these transitions to more fully determine the role that H_2 is playing in this object.

If the luminosity of HH 43 derives entirely from the kinetic energy of a collimated flow from IRS 1, we can estimate the mass flux in the flow. We find a value of $\dot{M} > 1.3 \times 10^{-7}\ M_\odot\ yr^{-1}$ where the lower limit results from assuming that the computed luminosity of .23 $L_\odot$ applies and that the entire kinetic energy of the flow (per sec) is converted into shock luminosity. If the collimated mass flux at velocity v passes through a shock front with effective area A, one can write

$$\dot{M} = n\bar{m}Av$$

where n is the gas number density in the pre-shock flow and $\bar{m}$ is the average mass per particle. With the lower limit to the mass flux $\dot{M}$, and using $n \approx 100$ cm^{-3} as an average pre-shock density, we find that the computed area (2.7×10^{33} cm^2) is roughly comparable to the observed area ($\sim 4 \times 10^{33}$ cm^2) of HH 43. Of course, the computed area is a lower limit since the luminosity used to obtain $\dot{M}$ is a lower limit. Also, the shock area as seen by the flow coming from the star may in general be somewhat different than the area of HH 43 as seen from earth, but probably not by a large amount. It is in fact clear that the mass flux in the flow must be considerably greater than the computed lower limit since 43 B and C possess substantial kinetic energy which must be added to the radiative luminosity in order to achieve a reliable estimate of the total energy of the flow.

We wish to express our thanks to the staffs of the I.U.E. and the A.A.T. for their help in the use of these most exceptional instruments. One of us (M.C.) acknowledges travel support granted by the Director of Kitt Peak National Observatory for travel to foreign observatories. This work was made possible in part by NASA grants NSG 5-243 and NSG 5-421, and in part by NSF grant AST 8201430.

References

Bohlin, R.C., and Savage, B.D. (1981). Astrophys. J. 249, 109.

Böhm, K.-H. and Böhm-Vitense, E. (1984). Astrophys. J. 277, 21[illegible].

Böhm, K.-H., Brugel, E.W., and Olmsted, E. (1983). Astron. Astrophys. 125, 23.

Boksenberg, A. (1972). Proc. ESO/CERN Conf. on Auxiliary Instrumentation for Large Telescopes, Geneva, May 2-5, p. 295.

Cohen, M., Harvey, P.M., Schwartz, R.D., and Wilking, B.A. (1984). Astrophys. J. 278, 671.

Cohen, M., and Schwartz, R.D. (1983). Astrophys. J. 265, 877.

Dopita, M.A., Binette, L., and Schwartz, R.D. (1982). Astrophys. J. 261, 183.

Hartmann, L., and Raymond, J.C. (1984). Astrophys. J. 276, 560.

Lee, T.A. (1968). Astrophys. J. 152, 913.

Miller, J.S. (1968). Astrophys. J. Lett. 154, L57.

Münch, G. (1983). Rev. Mex. Astron. Astrophys. 7, 229.

Norman, C.A., and Silk, J. (1979). Astrophys. J. 228, 197.

Savage, B.D., and Mathis, J.S. (1979). Ann. Rev. Astron. Astrophys. 17, 73.

Schwartz, R.D. (1978). Astrophys. J. 223, 884.

Schwartz, R.D. (1983). Astrophys. J. Lett. 268, L37.

Turnrose, B.E., Harvel, C.A., and Stone, D.F. (1981). International Ultraviolet Explorer Image Processing INfromation Manual, Version 1.1.

Table 1

HH 43 Ultraviolet Emission Lines

Ident.	λ(Å)	1982 F^1(Obs)	1984 F^1(Obs)	Mean F^1(Obs)	F_o[1,2]	I[3]	I[4]
H_2 1→3 R(3)	1257.8	0.51	0.45	0.48	1.7	77	142
H_2 1→3 P(5)	1271.9	1.20	0.90	1.05	3.7	168	172
H_2 1→6 R(3)	1431.0	0.98	0.83	0.91	3.0	136	128
H_2 1→6 P(5)	1446.1	1.30	1.20	1.25	4.3	195	157
H_2 1→7 R(3)	1489.6	1.00	1.40	1.20	3.9	177	180
H_2 1→7 P(5)	1504.8	1.50	1.40	1.45	4.9	222	222
H_2 1→8 R(3)	1547.4	0.60	0.62	0.61	2.0	91	116
H_2 1→8 P(5)	1562.4	1.30	0.59	0.95	3.2	145	140
C II]	2326		1.50	1.50	5.7	258	
[O II]	2470		0.20	0.20	0.76	34	
Mg II	2800		0.53	0.53	1.8	82	
C I]	2968		0.51	0.51	1.7	77	

[1,2] All fluxes in units of 10^{-13} erg cm^{-2} s^{-1}.
[2] Fluxes corrected for θ Ori extinction, E(B-V) = 0.2, R = 5.
[3] Mean intensities normalized to I(Hβ) = 100.
[4] Theoretical intensities (Dopita, unpublished) normalized to the observed intensity of the λ 1504.8 line.

Table 2

HH 43 Ultraviolet Continuum Fluxes

λ(Å)	$\frac{1}{\lambda}(\mu^{-1})$	F_λ[1](Obs)	F_λ[1,2]	λ(Å)	$\frac{1}{\lambda}(\mu^{-1})$	F_λ[1](Obs)	F_λ[1,2]
1250	8.00	5.42	19.14	2200	4.55	2.82	12.31
1300	7.69	6.30	21.64	2250	4.44	3.05	12.95
1350	7.41	4.34	14.64	2300	4.35	2.00	8.26
1400	7.14	4.43	14.67	2350	4.26	2.36	9.48
1450	6.90	5.12	16.80	2400	4.17	2.32	9.07
1500	6.67	7.10	23.08	2450	4.08	2.29	8.71
1550	6.45	7.06	22.95	2500	4.00	2.04	7.61
1600	6.25	7.92	26.23	2550	3.92	2.06	7.55
1650	6.06	3.88	12.97	2600	3.85	2.31	8.39
1700	5.88	4.88	16.61	2650	3.77	1.82	6.49
1750	5.71	4.90	16.83	2700	3.70	1.57	5.54
1800	5.56	4.01	14.03	2750	3.64	1.54	5.39
1850	5.41	3.42	12.30	2800	3.57	1.42	4.92
1900	5.26	3.46	12.80	2850	3.51	1.40	4.81
1950	5.13	2.26	8.59	2900	3.51	1.40	4.83
2000	5.00	2.36	9.31	2950	3.39	1.54	5.19
2050	4.88	2.79	11.42	3000	3.33	1.58	5.28
2100	4.76	3.96	16.81	3050	3.28	1.31	4.38
2150	4.65	4.51	19.69	3100	3.23	1.23	4.07

[1] Fluxes in units of 10^{-15} erg cm^{-2} s^{-1} Å^{-1}.
[2] Fluxes corrected for θ Ori extinction, E(B-V) = 0.2, R = 5.

Table 3

HH 43 Optical Emission Lines

Ident.	λ(Å)	1984 43A	1984 43B	1984 43C	1984 A+B+C	1981 A+B+C	$\bar{I}$	I_o[1]
[O II]	3727	153.1	117.6	50.4	106.3	96.2	99.6	113.3
Ca II	3933		7.8	14.1	8.2	7.8	7.9	8.8
Ca II+Hε	3969		18.0	14.1	14.2	13.4	13.7	15.3
[S II]	4068/76		66.1	95.3	63.1	61.3	61.9	68.5
Hδ	4101		18.4	8.7	13.0	15.4	14.6	16.1
Hγ	4340	40.7	35.5	41.0	37.7	37.2	37.4	40.6
[Fe II]+[O III]	4363	22.7	2.6		5.1	5.6	5.4	5.8
Mg I]	4571		15.4	21.3	14.5	14.5	14.5	15.2
Hβ	4861	100.0	100.0	100.0	100.0	100.0	100.0	100.0
[O III]	4959	18.1			2.8	1.7	2.1	2.1
[O III]	5007	54.2			8.5	5.6	6.6	6.4
[Fe II]	5158	10.3	8.2		6.5	7.5	7.2	6.9
[N I]	5199	19.8	114.3	152.3	109.0	120.6	116.7	111.2
[O I]	6300	86.3	348.8	404.7	322.2	452.5	409.1	340.3
[O I]	6363	25.2	113.3	134.4	104.7	147.3	133.1	109.7
Hα	6563	493.1	501.7	392.2	473.5	575.0	541.2	437.9
[N II]	6583	140.5	104.3	73.3	102.2	120.6	114.5	90.1
[S II]	6717	138.0	445.2	473.4	404.7	464.8	444.8	343.7
[S II]	6731	80.4	375.4	516.4	365.4	450.6	422.2	326.2
[Ca II]	7291		22.0	18.0	17.8	19.4	18.9	13.0
[O II]	7319		6.3					
[Ca II]	7325		19.0	15.2	18.8	18.4	18.5	12.7
[O II]	7330							
log F(Hβ)		-14.10	-13.52	-13.89	-13.29	-13.45	-13.10[2]	-12.66
Radial Velocity[3]		+44±28	-34±19	-143±21				

[1] Line intensities corrected for θ Ori extinction, E(B-V) = 0.2, R = 5.
[2] Mean of 1981 and 1984 fluxes multiplied by the factor 1.83 required to normalize the optical continuum fluxes to the ultraviolet continuum fluxes.
[3] Heliocentric radial velocity in km s^{-1}.

Table 4

HH 43 Optical Continuum Fluxes

λ(Å)	$\frac{1}{\lambda}(\mu^{-1})$	F_λ [1](Obs)	F_λ [1,2]	λ(Å)	$\frac{1}{\lambda}(\mu^{-1})$	F_λ [1](Obs)	F_λ [1,2]
3390	2.95	1.03[3]	3.32[3]	4830	2.07	0.321	0.91
3500	2.86	0.82	2.61	5080	1.97	0.31	0.84
3600	2.78	0.76	2.39	5230	1.91	0.29	0.75
3910	2.56	0.53	1.63	5470	1.83	0.23	0.60
4000	2.50	0.49	1.50	5650	1.77	0.22	0.60
4170	2.40	0.49	1.50	5650	1.77	0.22	0.56
4520	2.21	0.38	1.11	6000	1.67	0.21	0.48
4620	2.16	0.34	0.98	6200	1.61	0.20	0.44

[1] Fluxes in units of 10^{-15} erg cm^{-2} s^{-1} Å^{-1}.
[2] Fluxes corrected for Θ Ori extinction, E(B-V) = 0.2, R = 5.
[3] 1981 flux only

Figure Captions

Figure 1. A sketch of HH 43 and the position of the exciting star IRS 1 (Cohen and Schwartz 1983). The faint star lying near the southwest side of HH 43 is an unrelated foreground star.

Figure 2. The spectrum of HH 43 obtained with the I.U.E. (LWP 4041) on 19 August 1984. The spectrum is uncorrected for extinction with a 5-point smoothing function applied. The "X's" denote regions where camera defects have been removed. For $\lambda < 2300$Å, the sensitivity of the LWP system decreases rapidly, and the apparent line structure is the result of the gaussian smoothing of noise.

Figure 3a. The spectrophotometric tracing (corrected for atmospheric extinction) of HH 43 A obtained with the A.A.T. Note the clear presence of [O III] λ 5007 and the very weak [N I] λ 5200 emission.

Figure 3b. Spectrophotometry of HH 43 B. Note the disappearance of [O III] and the dramatic appearance of [N I]. This occurs in one pixel step (~ 2").

Figure 3c. Spectrophotometry of HH 43 C. All fluxes in Fig. 3 are in ergs cm^{-2} s^{-1}.

Figure 4. The combined UV ($1/\lambda > 3.23$) and optical ($1/\lambda < 2.95$) continuum fluxes summed over all components of HH 43. The observed fluxes have been corrected for normal (Savage and Mathis 1979) extinction assuming E(B-V) = 0.46. The dashed line is the theoretical two-photon distribution, and the solid line the combined two-photon and free-bound continua as discussed in Dopita et al. 1982.

Figure 5. As in Fig. 4, except the Θ Ori extinction curve (Bohlin and Savage 1981) with E(B-V) = 0.46, R = 5 has been applied to all data points.

Figure 6. As in Fig. 4, except the θ Ori extinction curve with E(B-V) = 0.2, R = 5 has been applied to the observed continuum fluxes.

Figure 7. Comparison of the normal and peculiar (θ Ori) extinction curves. HH 43 fluxes appear to be consistent with correction by the dashed-line which closely parallels θ Ori extinction.

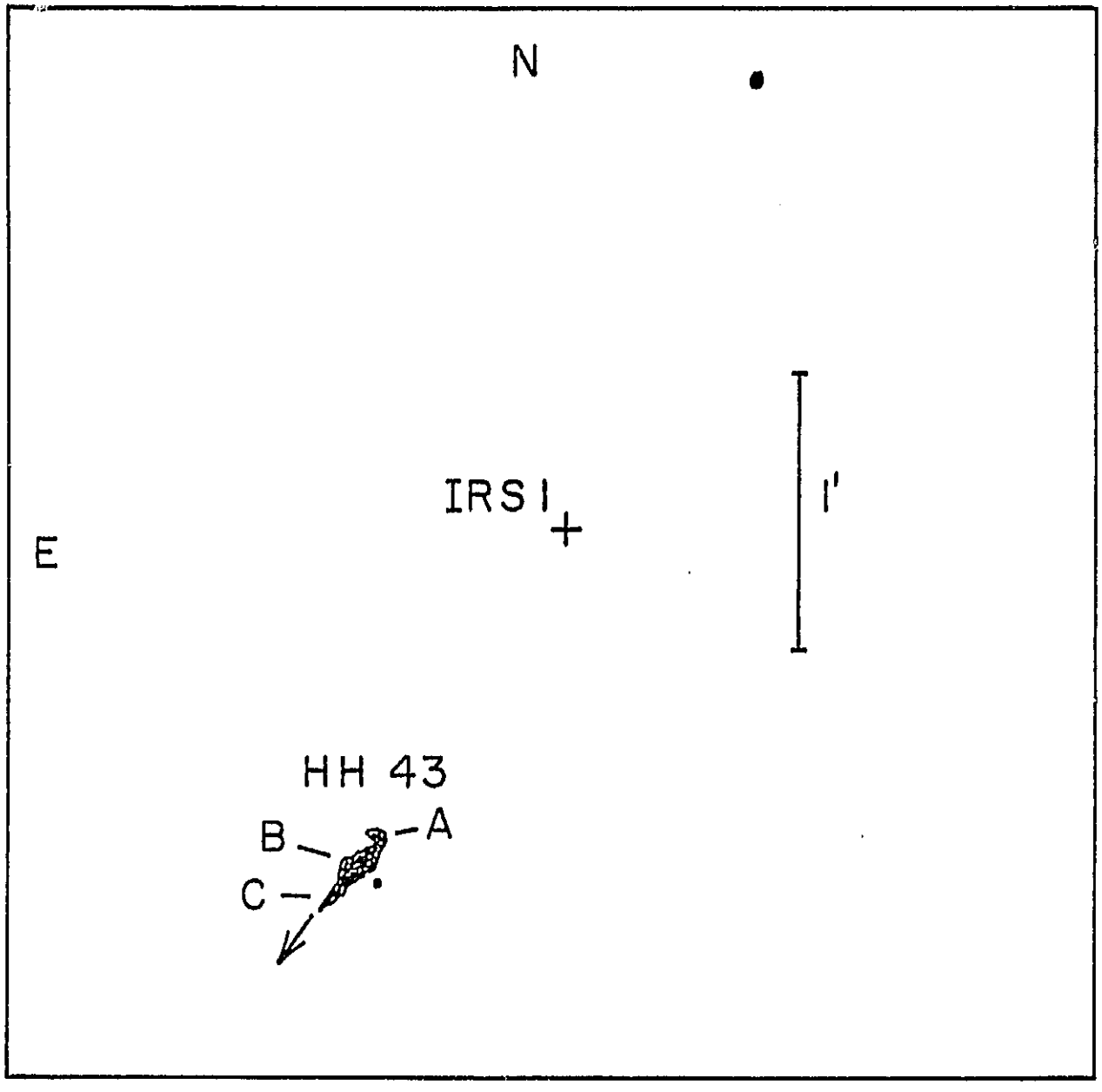
N
IRS 1
1'
E
HH 43
B
A
C

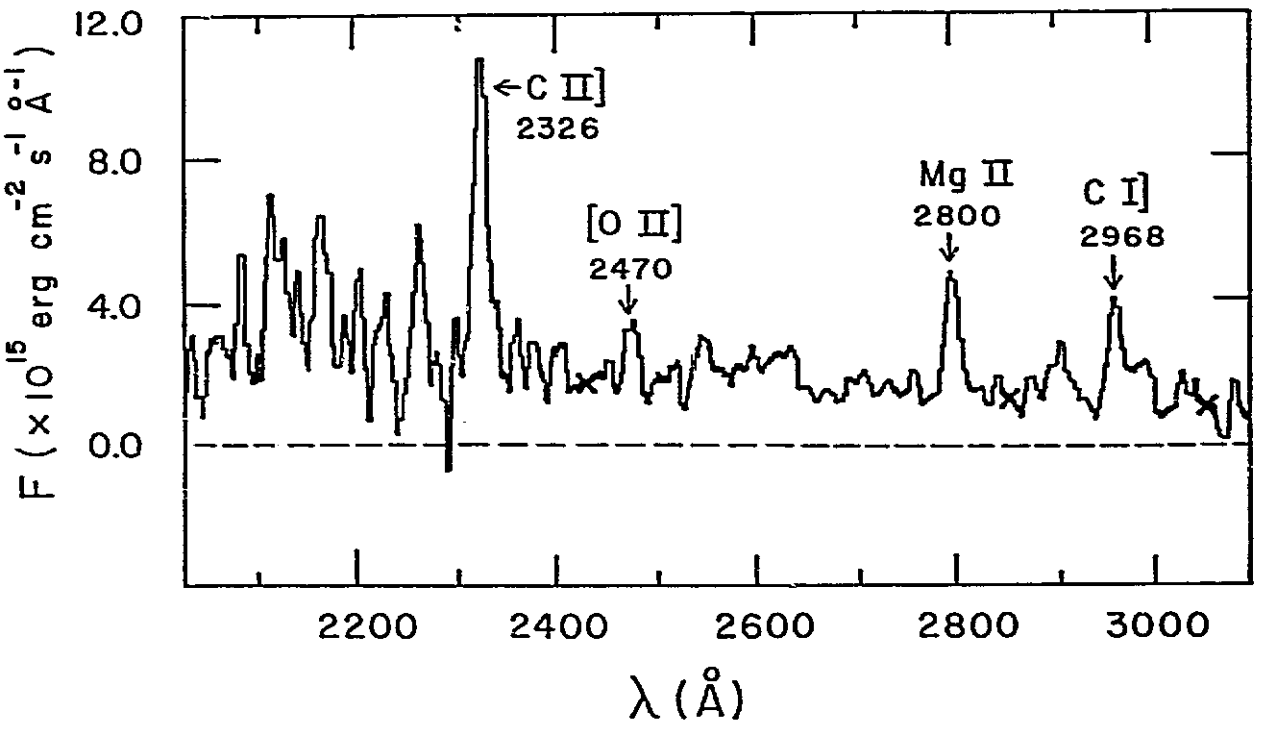
12.0
8.0
4.0
0.0
F (x 10^15 erg cm^-2 s^-1 Å^-1)
←C II]
2326
[O II]
2470
Mg II
2800
C I]
2968
2200
2400
2600
2800
3000
λ (Å)

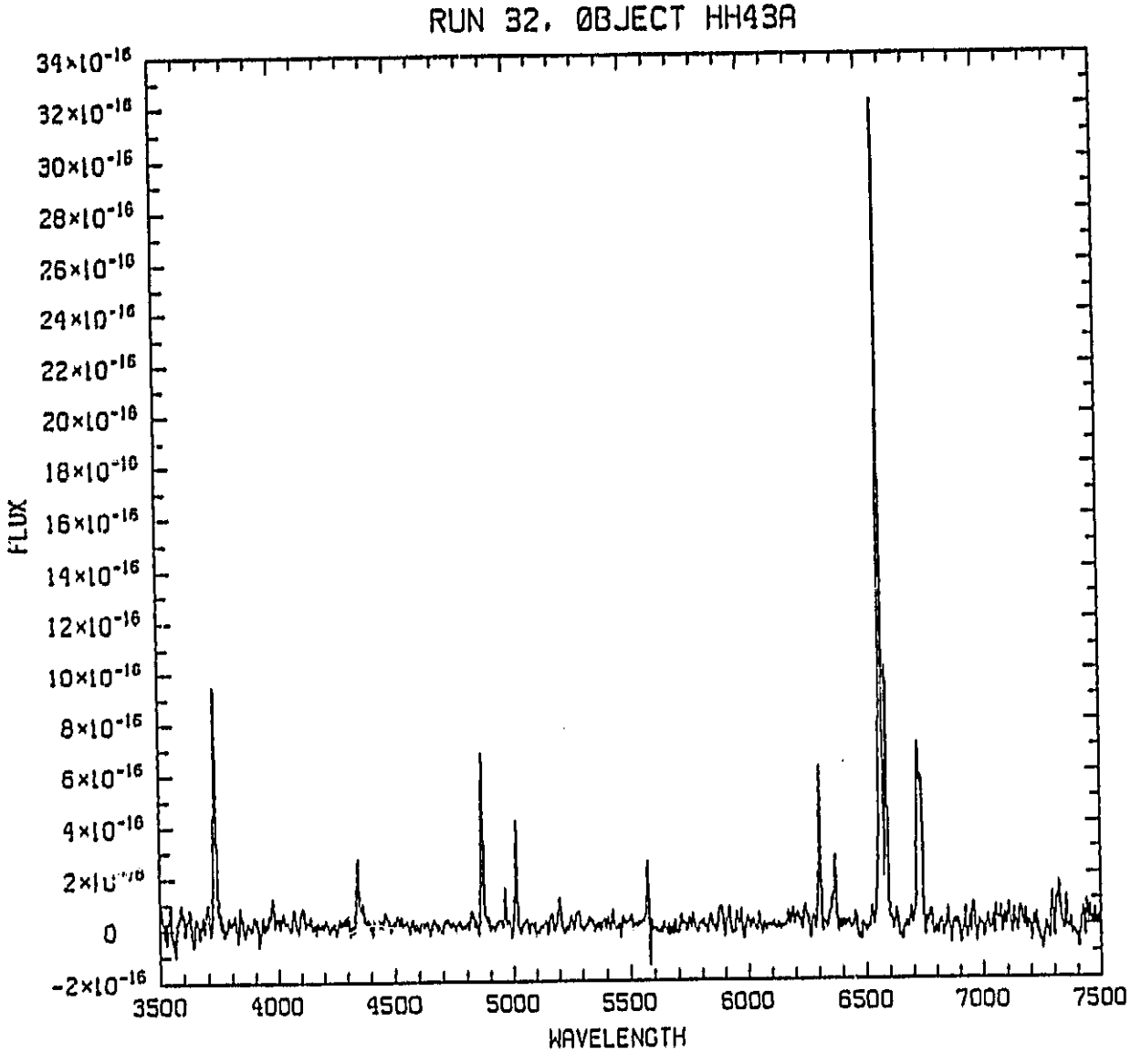
RUN 32. OBJECT HH43A
FLUX
WAVELENGTH
34x10-16
32x10-16
30x10-16
28x10-16
26x10-16
24x10-16
22x10-16
20x10-16
18x10-16
16x10-16
14x10-16
12x10-16
10x10-16
8x10-16
6x10-16
4x10-16
0
-2x10-16
3500
4000
4500
5000
5500
6000
6500
7000
7500

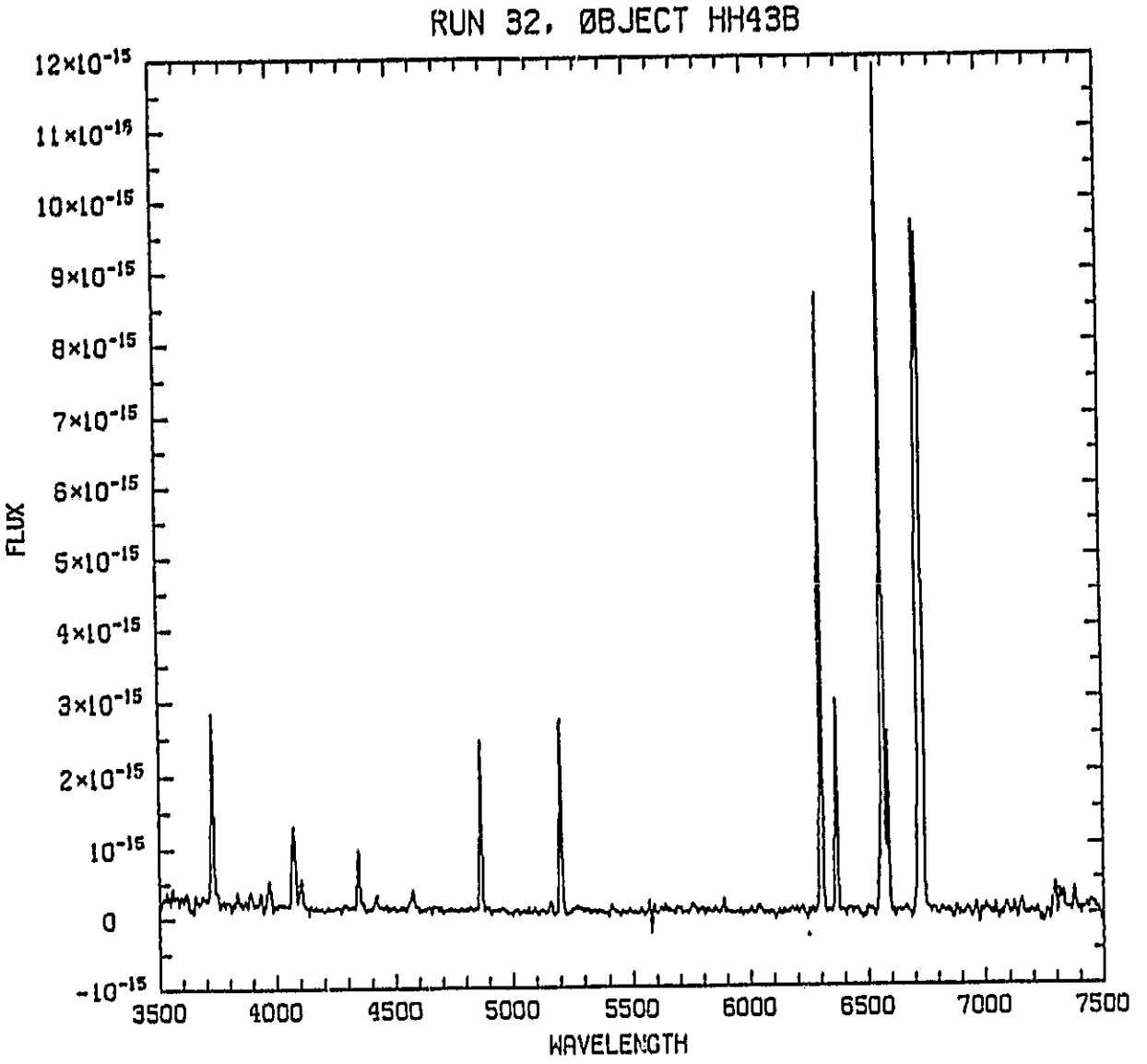
RUN 32, ØBJECT HH43B
12×10⁻¹⁵
11×10⁻¹⁵
10×10⁻¹⁵
9×10⁻¹⁵
8×10⁻¹⁵
7×10⁻¹⁵
6×10⁻¹⁵
5×10⁻¹⁵
4×10⁻¹⁵
3×10⁻¹⁵
2×10⁻¹⁵
10⁻¹⁵
0
-10⁻¹⁵
FLUX
3500
4000
4500
5000
5500
6000
6500
7000
7500
WAVELENGTH

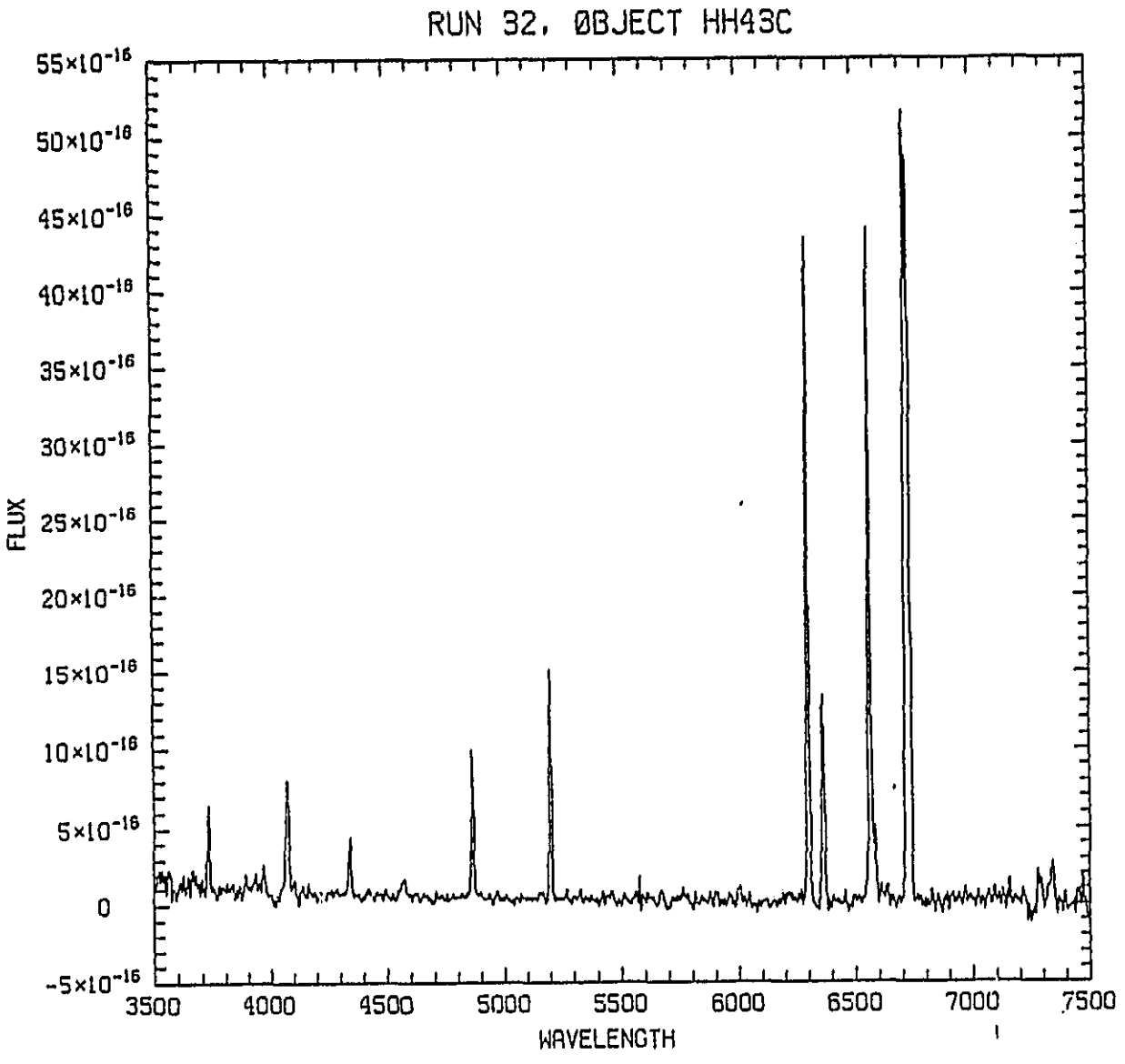
RUN 32. ØBJECT HH43C
55×10⁻¹⁶
50×10⁻¹⁶
45×10⁻¹⁶
40×10⁻¹⁶
35×10⁻¹⁶
30×10⁻¹⁶
25×10⁻¹⁶
20×10⁻¹⁶
15×10⁻¹⁶
10×10⁻¹⁶
5×10⁻¹⁶
0
-5×10⁻¹⁶
FLUX
3500
4000
4500
5000
5500
6000
6500
7000
7500
WAVELENGTH

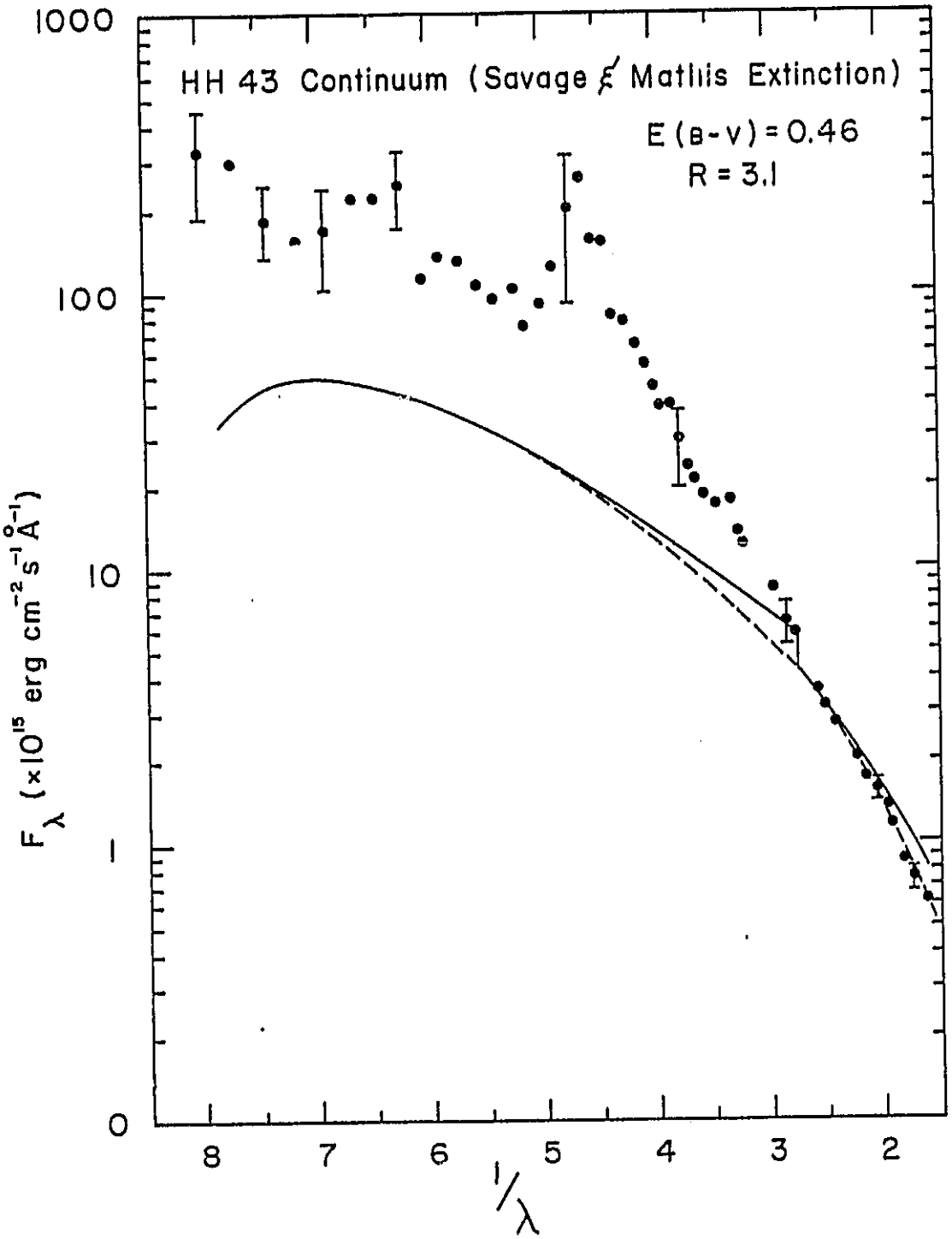
HH 43 Continuum (Savage & Mathis Extinction)
E(B-V) = 0.46
R = 3.1
1000
100
10
1
0
8
7
6
5
4
3
2
1/λ
F_λ ($\times 10^{15}$ erg cm^{-2} s^{-1} Å^{-1})

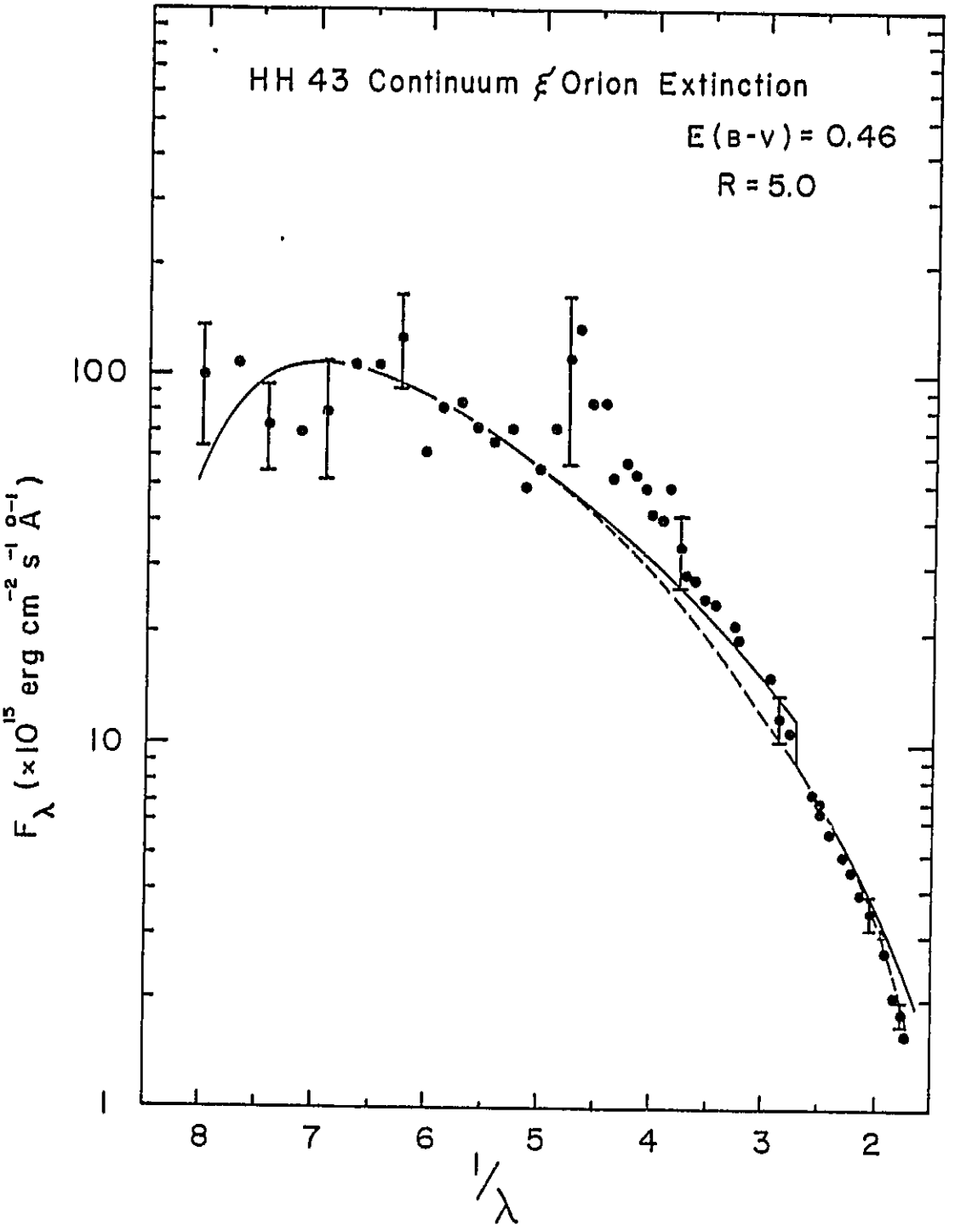
HH 43 Continuum & Orion Extinction
E(B-V) = 0.46
R = 5.0
100
10
1
8
7
6
5
4
3
2
1/λ
F_λ ($\times 10^{15}$ erg cm^{-2} s^{-1} Å^{-1})

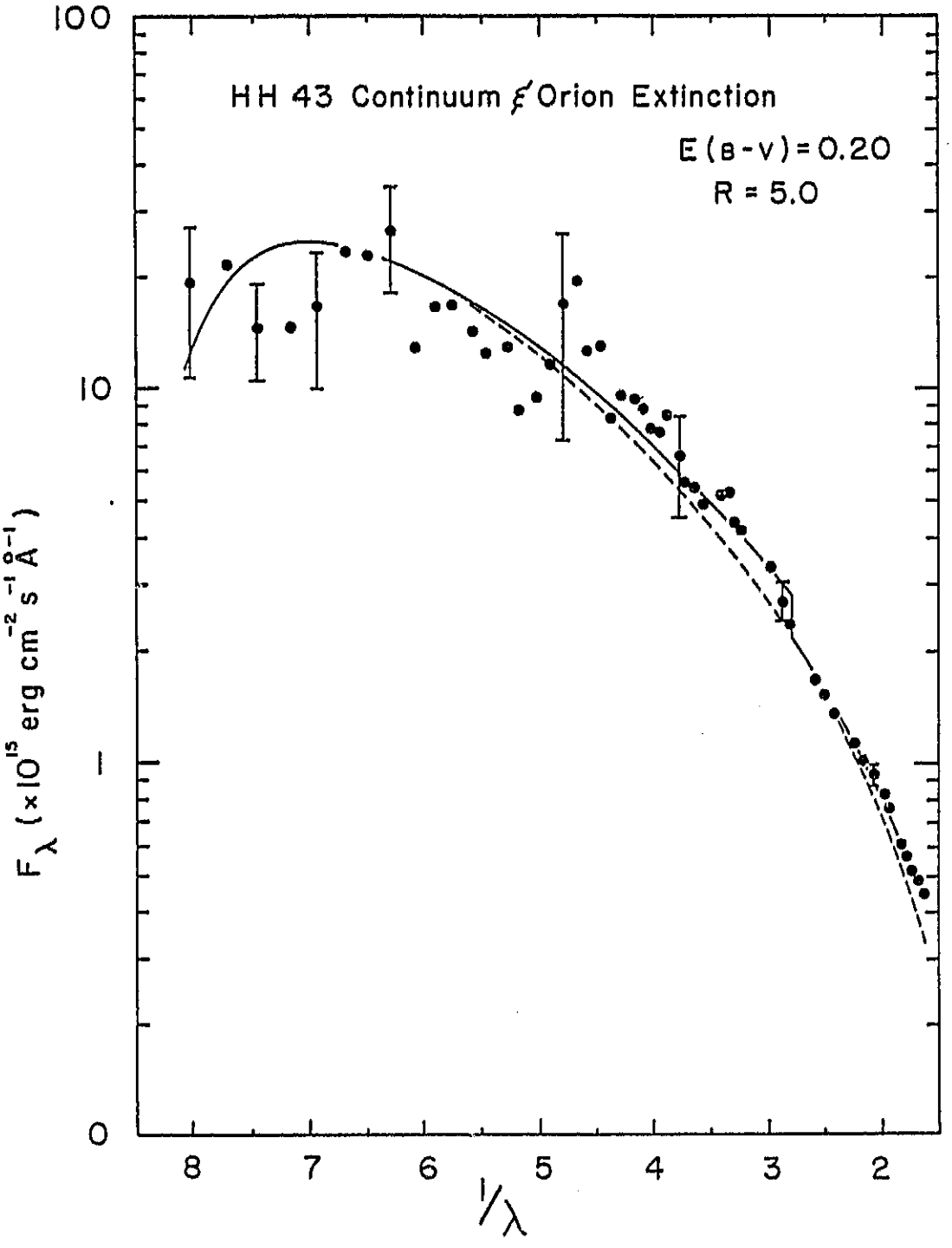
HH 43 Continuum & Orion Extinction
E(B-V) = 0.20
R = 5.0
100
10
1
0
8
7
6
5
4
3
2
1/λ
F_λ ($\times 10^{15}$ erg cm^{-2} s^{-1} Å^{-1})

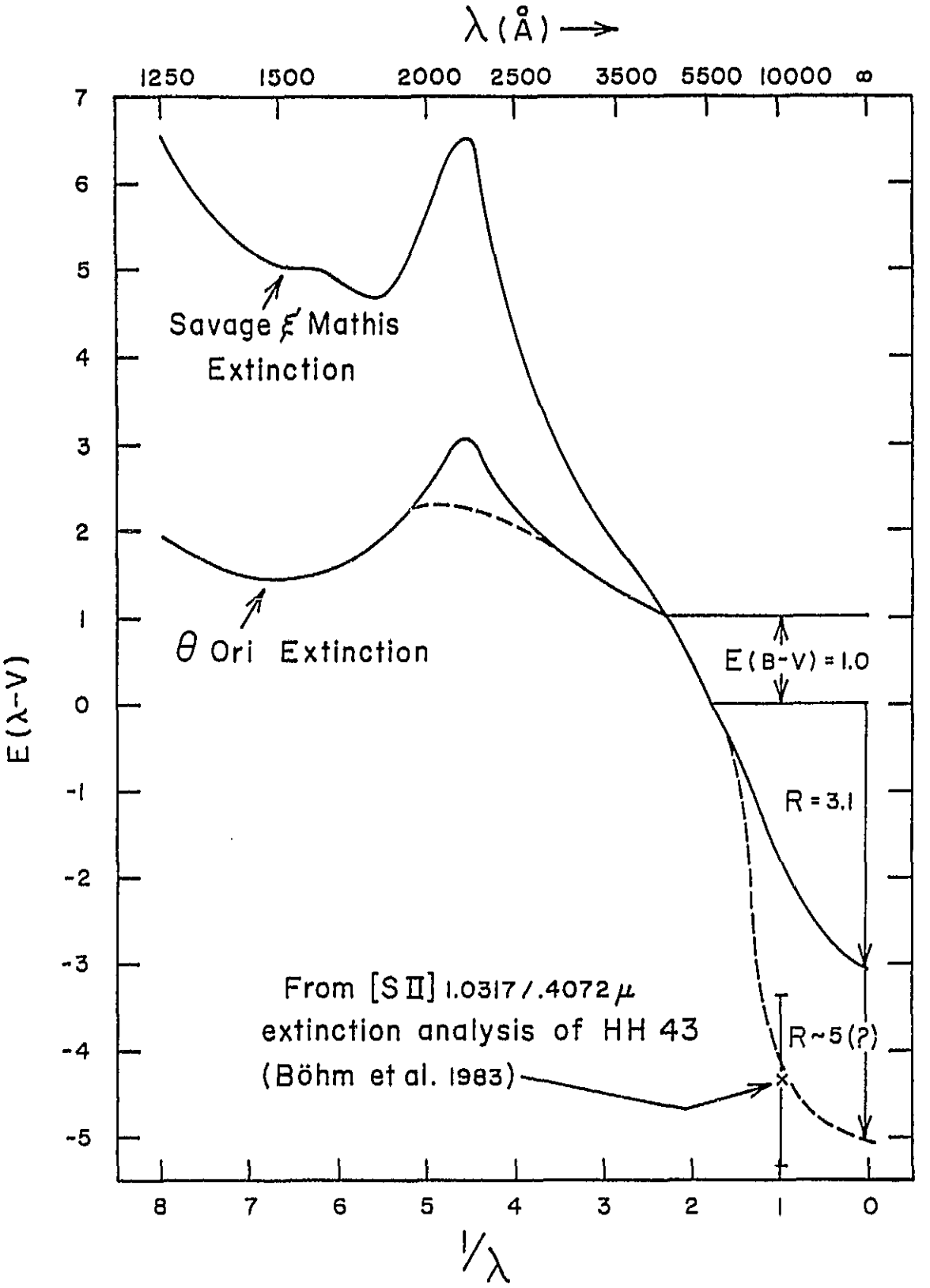
λ (Å) →
1250
1500
2000
2500
3500
5500
10000
∞
7
6
5
4
3
2
1
0
-1
-2
-3
-4
-5
E(λ-V)
Savage & Mathis Extinction
θ Ori Extinction
E(B-V) = 1.0
R = 3.1
From [S II] 1.0317/.4072 μ
extinction analysis of HH 43
(Böhm et al. 1983)
R~5(?)
8
7
6
5
4
3
2
1
0
1/λ